THE JOURNAL OF PHYSICAL CHEMISTRY C

Article

pubs.acs.org/JPCC

Understanding the Effects of Ion-Exchange in Titanosilicate ETS-10: A Joint Theoretical and Experimental Study

Mehmet Koç,[†] Sezin Galioglu,[†] Daniele Toffoli,*[,§] Hande Ustunel,*[,⊥] and Burcu Akata*[,†,‡]

[†]Micro and Nanotechnology Department, Middle East Technical University, 06800 Ankara, Turkey

[‡]Central Laboratory, Middle East Technical University, 06800 Ankara, Turkey

[§]Department of Chemistry, Middle East Technical University, 06800 Ankara, Turkey

[⊥]Department of Physics, Middle East Technical University, 06800 Ankara, Turkey

Supporting Information

ABSTRACT: Density functional theory (DFT) calculations within the gradient-corrected approximation (GGA) were carried out on two models of Engelhard titanosilicate (ETS-10) with the aim to elucidate the effect of ion exchange on the structural and electronic properties of the Ti−O−Ti quantum wire. The partial and full exchange of Na^+ cations with alkaline, earth-alkaline, and transition metal ions have been investigated. The theoretical results have been complemented by experimental X-ray diffraction (XRD) and Raman data in the region of the Ti−O−Ti stretching of the wire. Overall, the experimental data support the theoretical findings where substitution of Na^+ with K^+, Ag^+, and Ca^{2+} cause only minor structural changes in the wire while the inclusion of Zn^{2+}, Ru^{3+}, and Au^{3+} cause its partial or entire disruption.

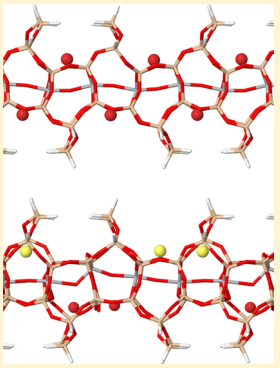

1. INTRODUCTION

A fairly new member of the zeolite family, Engelhard titanosilicate (ETS-10) is a synthetic microporous crystalline material (pore dimensions 4.9 and 7.6 Å) whose framework structure results from chains of corner-sharing TiO_6 octahedra and SiO_4 tetrahedra linked through bridging oxygen atoms[1,2] generating a pore structure with 12-membered rings. Although the material is crystalline, its structural determination has proven to be challenging.[3] The ETS-10 structure can be described in terms of two ideal polymorphs. Polymorph A has a tetragonal crystal structure (space group $P4_1$ or $P4_3$), while polymorph B belongs to the monoclinic system (space group $C2/c$). The main difference between the two polymorphs is the stacking sequence of the unit cell along the [001] direction: polymorph A has zigzag channels, while the polymorph B structure is characterized by a diagonal stacking arrangement.[4,5] In the real material, an intergrowth of both polymorphs is responsible for its disorder due to such irregularities as stacking faults and line defects. An intriguing characteristic of ETS-10 is that TiO_6 octahedra are linked together to form −Ti−O−Ti− wires running in the crystal along the [100] and [010] directions.[2] These linear chains are effectively insulated by the silica matrix and can be regarded as a 1-D quantum-confined form of titania[6] whose band gap depends on the length of the crystals along the [110] direction.[7] Two of the six oxygen atoms in each TiO_6 unit lie along the wire and four in a plane perpendicular to the wire axis surrounding the central Ti atom. The former are thus referred to as *apical* oxygens (O_{ap}) while the latter as *equatorial* (O_{eq}).

In the native form of ETS-10 ($(Na,K)_2TiSi_5O_{13}$[2,3]), extra-framework Na^+ and K^+ cations compensate the two negative charges of each TiO_6^{2-} unit. As a part of the search for the detailed structure of the material, several theoretical studies have focused on the location of the extra-framework cations. According to an earlier ab initio investigation by Ching et al.,[8] the Na^+ cations are likely to be located only in the seven-membered ring pores, at different distances from the titanium atoms. In the work of Grillo and Carrazza,[9] four different cation sites have been identified for both Na^+ and K^+ cations; the sites are distributed along the Ti−O−Ti wire, surrounded by silicon five-rings and between two vicinal Ti atoms of the wire. In a subsequent joint theoretical and experimental NMR study, Anderson et al.[10] identified five different cation sites, where sites I, II, and III are in agreement with the corresponding locations identified by Grillo et al.[9] The Hartree−Fock (HF) and periodic density functional theory (DFT) calculations of Damin et al.[4] also agree with the results of Grillo et al. concerning the position of the Na^+ cations. These cations can be exchanged with other cations through ion exchange in aqueous solutions. The ion exchange is however responsible for local damage of the ETS-10 structure.[11−13]

Due to the variety of applications that ETS-10 presents, several theoretical and experimental studies have been devoted to the elucidation of the structural, electronic, and vibrational

Received: April 20, 2014
Revised: November 6, 2014
Published: November 6, 2014

properties of ETS-10[3−6,8,14−20] over the last two decades. The UV−vis spectrum of ETS-10 (Na-form) is characterized by two intense absorption bands, with maxima at 4.4 and 5.8 eV.[21] Both bands have been assigned to ligand-to-metal charge transfer (LMCT) transitions, which differ depending on the types of oxygen ligands involved. The LMCT transition at 5.8 eV involves the equatorial oxygens around the Ti−O−Ti wire and is therefore localized in a single TiO_6 unit, while the transition at 4.4 eV (with an inflection point at 4.02 eV[21]) is delocalized over large distances along the quantum wire.[6,15,21]

Theoretical estimates of the ETS-10 band gap vary between different sources depending on the method and the model used. First-principles calculations performed by Ching et al. give a band gap value of 2.33 eV,[8] while a value of 3.95 eV, in rather good agreement with the experiment, has been reported by Bordiga et al.[15] in the local density approximation (LDA) using a simplified model of ETS-10. On the basis of their QM/MM studies, Zimmerman et al. reported an estimated optical band gap of about 3.0 eV,[5] in close agreement with the LDA band gap estimate of Damin et al.,[4] with a value of 3.22 eV. These studies all agree on the major atomic orbital contributions to the top of the valence band (O 2p orbitals) and the bottom of the conduction band (Ti 3d orbitals), therefore supporting the earlier study of Borello et al.[21] Due to quantum confinement effects, the band gap is blue-shifted by about 0.8−1.0 eV with respect to the correspondent E_g value of bulk rutile (3.02 eV) and anatase (3.18 eV). Furthermore, the band gap energy is not appreciably affected by cation exchange (maximum variation of the order of 5%[6]).

The potential use and performance of ETS-10 titanosilicate in a variety of different applications is directly related to its unique Ti−O−Ti wire. Attaining atomistic information on its structural and electronic properties is very useful for tailoring and expanding its potential applications, which already cover a broad range due to its well-known catalytic selectivity[22−24] and photoreactivity.[25] Moreover, promising applications include the removal of harmful heavy-metal ions,[11−13,26,27] dye sensitized solar cells,[28] and photochromism.[29] In this respect, the ability to tune and modify in a controllable way the properties of the quantum wire can lead toward enhancements in applications of molecular-wire superlattices in nanoscale electronic devices.[7]

Raman spectroscopy is a valuable tool for the study of structural defects of the Ti−O−Ti quantum wire in ETS-10.[7,11,13,30,31] A strong band at about 725 cm^{-1} dominates the experimental Raman spectrum and has been assigned to lateral Ti−O−Ti stretching in the wire.[4,30] Its frequency, width, and intensity are related to the average length, length homogeneity, and concentration of defects in the Ti−O−Ti chains.[7] Therefore, the changes induced in the 725 cm^{-1} band give definitive clues on the partial or entire disruption of the Ti−O−Ti chains in the ETS-10.[11,13,17]

The octahedral arrangements of the oxygen ligands around each Ti^{4+} center is distorted. The distance between Ti atoms and the four oxygens bridging Ti and Si atoms (O_{eq}) is in the range of 2.00−2.10 Å.[18,19] In spite of general consensus, some conflicts still exist concerning the Ti−O bond lengths along the quantum wire. In an earlier study, Sankar et al.,[18] were able to obtain a satisfactory fit of their EXAFS data with a model characterized by two nonequivalent Ti−O bonds along the chain (with Ti−O distances of 1.71 and 2.11 Å), and with a Ti−O−Ti bond angle of 165°, in disagreement with other experimental[3,19] and theoretical studies,[4] all suggesting equal Ti−O bond lengths along the chain, together with a Ti−O−Ti bond angle much closer to 180°.

In this paper, we carried out a joint experimental and theoretical study of the structural, electronic, and vibrational properties of ETS-10 (Na-form) and fully and partially ion-exchanged M-ETS-10 (M = K^+, Ag^+, Ca^{2+}, Zn^{2+}, Ru^{3+}, and Au^{3+}). Theoretical calculations were carried out using DFT on two ETS-10 model systems and were supported by X-ray diffraction (XRD) and Raman spectroscopy measurements. The aim was to systematically investigate the extent of local structural changes caused by the exchange of Na^+ and K^+ with a large selection of metal ions, from Ca^{2+}, which is seen to not alter the electronic/structural properties of the wire, to Zn^{2+}, Ru^{3+} and Au^{3+}, which progressively cause extensive modifications. It is suggested that ion-exchange can be used to tune the structural/electronic properties of ETS-10 by carefully choosing the most appropriate ion and the degree of exchange.

The plan of the paper is as follows. In section 2, we describe our computational and experimental method. Our results are presented in section 3, while conclusions and perspectives follow in the final section 4.

2. COMPUTATIONAL AND EXPERIMENTAL DETAILS

The calculations were performed using plane-wave pseudopotential density functional theory[32,33] with the gradient-corrected approximation (GGA) and ultrasoft pseudopotentials[34] to model electron−ion interaction. The Perdew−Becke−Ernzerhof[35] exchange-correlation functional as implemented in the Quantum-Espresso distribution[36] was used in all calculations. The open-source programs XCrysDen[37] and Jmol[38] were used for visualization and to produce the figures, respectively.

During the BFGS geometry optimizations, a force threshold per atom of 0.025 eV/Å was used and all atomic coordinates were allowed to relax. The plane-wave basis set is defined by a kinetic energy cutoff of 35 Ryd, while the charge density cutoff is 350 Ryd. For both models of ETS-10 considered in the present study, atomic positions and the cell parameter a have been taken from the experimental data of Anderson et al.,[2] corresponding to polymorph A (cell parameters $a = b = 14.85$ Å and $c = 27.08$ Å). Due to the large number of atoms in the full primitive unit cell, two models were employed that are built on a single quantum wire with varying degrees of the surrounding framework. Such a reduced representation is justified owing to the importance of the wire in determining the relevant properties of ETS-10. Our larger model, model II, is shown in Figure 1, where the atomic labeling used in the following discussion is introduced. The two models are compared in Figure 2. Model I is similar to the corresponding model I used by Damin et al.,[4] with two Ti atoms in the repeating unit and the surrounding silica matrix atoms. Model II is instead characterized by four Ti atoms and a larger number of framework atoms in the repeating unit. In particular, model II has a fully formed seven-membered ring above the Ti−O−Ti wire in contrast to the partial representation in the model of ref 4 and model I. Furthermore, the length of the repeating unit of model II is twice that of model I due to the periodicity of the seven-membered rings. Both models are hydrogen-terminated to saturate the dangling bonds, and the positions of the hydrogen atoms have been kept fixed during geometry optimization. The minimum distance between periodic images in all systems considered is approximately 12 Å. For both models, the extraframework Na^+ cations are explicitly included for charge neutrality.

dx.doi.org/10.1021/jp503852t | J. Phys. Chem. C 2014, 118, 27281−27291

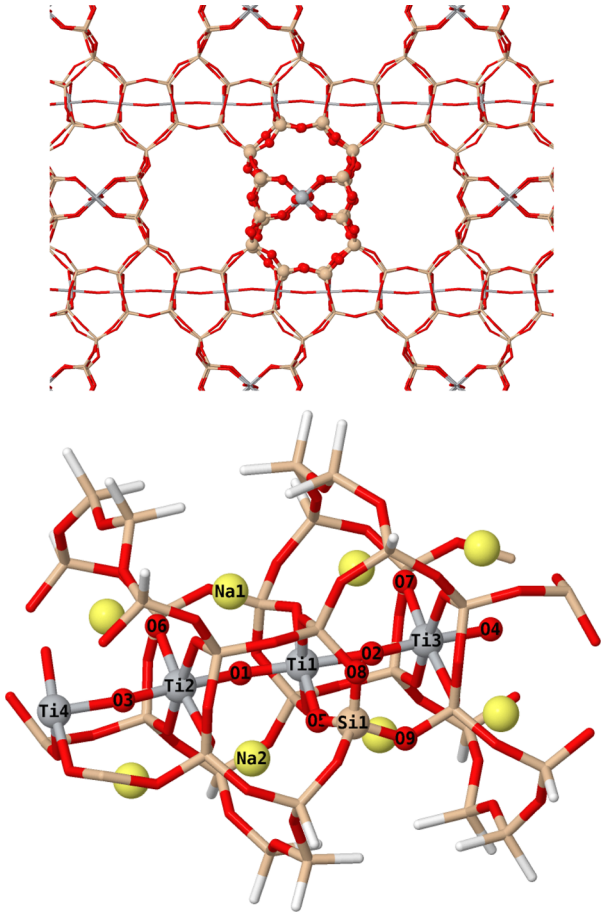

Figure 1. Na-ETS-10 model II with atomic labels referred to in the text.

The charge on each exchanged ion is different, and therefore full cation exchange was simulated in the following way. In the case of the singly charged cations (K^+ and Ag^+), each Na^+ ion was replaced with one cation (top two panels of Figure 3) while the doubly charged ions (Ca^{2+} and Zn^{2+}) each replace two Na^+ ions in a *zigzag* geometry (lower two panels of Figure 3). Finally, six Na^+ atoms were removed and replaced with two ions in the case of triply charged cations (Au^{3+} and Ru^{3+}). In this final case, in order to maintain charge neutrality, two Na^+ ions were left in the unit cell. In the case of Au^{3+}, two geometries, *zigzag* and *dimer-like*, were studied, where the Au^{3+} ions were placed on opposite sides and on the same side of the wire, respectively (Figure 4). Partial cation exchange was realized in a similar manner, where only one cation was introduced in each simulation cell, replacing as many Na^+ ions as were necessary to keep the structure neutral (see Figure 5 and Figure 6). Geometry optimizations and total energy calculations were performed with a $1 \times 8 \times 1$ ($1 \times 16 \times 1$ for model I) Monkhorst–Pack[39] k-point mesh, and a Gaussian smearing with a width of 0.01 Ryd was used in the Brillouin zone integration. Spin polarization was used as needed: of the two full exchange configurations considered for Au, the dimer configuration is spin unpolarized while the zigzag configuration has a magnetic moment of 2 μ_B. Similarly, the fully relaxed, fully exchanged Ru-form has a magnetic moment of 2 μ_B. The partially exchanged Au and Ru forms are both spin polarized with magnetic moments of about 2 μ_B and 1 μ_B, respectively. The spin-polarization of Ag atoms, for both partially and fully exchanged ETS-10, is zero. Partial charges were computed using a Bader charge analysis.[40]

The synthesis and characterization of the Na-ETS-10 and ion-exchanged ETS-10 (M-ETS-10) samples were conducted using the following protocol. All commercially obtained compounds for the preparation and synthesis of the samples were used as received: TiO_2 (P25, 76 wt % anatase and 24 wt % rutile, Degussa), $NaSiO_2$ were obtained from Sigma-Aldrich. $AgNO_3$(99.9%), NaCl (99.0%), KCl (99.0%), and H_2SO_4 (96.5%) were received from J. T. Baker, while $AuCl_3$ (99.0%) and $RuCl_3$(99.0%) were purchased from Aldrich. Zinc sulfate heptahydrate (99.0%) and calcium chloride dihydrate (99.0%) were received from Merck. Deionized water was distilled by a water purification system (Milli-Q system). All glassware and Teflon coated magnetic stir bars were cleaned with acetone, followed by copious rinsing with distilled water before drying in an oven at 373 K.

ETS-10 crystals were synthesized by using a molar composition of $3.4Na_2O{:}1.5K_2O{:}TiO_2{:}5.5\ SiO_2{:}150H_2O$.[13] In this preparation protocol, NaCl and KCl were dissolved in deionized water in a bottle. After dissolving these components, a sodium silicate solution was added and hand-shaken for 5 min, forming the Si precursor solution. For the preparation of the Ti precursor solution, H_2SO_4 was added to deionized water in a separate bottle. To this, P25 TiO_2 was added and hand-shaken for 5 min. After both precursor solutions were hand-mixed, the Ti precursor solution was poured into the Si precursor solution. The resulting mixture was hand-shaken for 5 min. The mixture was then transferred into Teflon-lined stainless steel autoclaves. The static synthesis was carried out for 3 days at 503 K; the products were cooled to room temperature, centrifuged, washed with deionized water, and dried overnight in ambient air at ~343 K. The M-ETS-10 were prepared by adding 400 mg of as-synthesized ETS-10 crystals

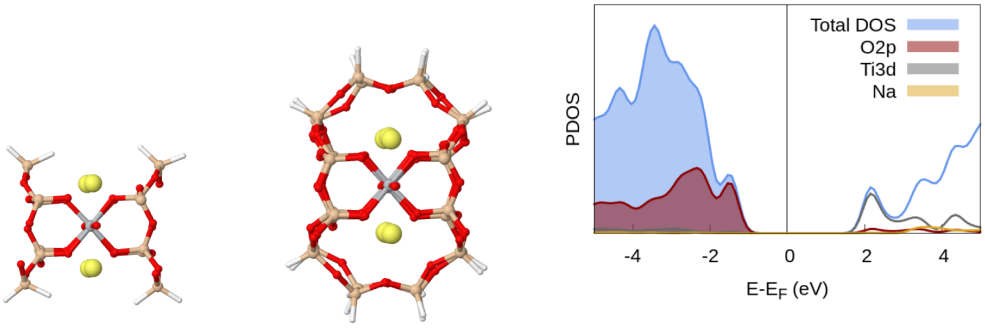

Figure 2. Model I (left) and model II (center) of Na-ETS-10. The partial density of states (PDOS) analysis for model II is included (right).

dx.doi.org/10.1021/jp503852t | J. Phys. Chem. C 2014, 118, 27281–27291

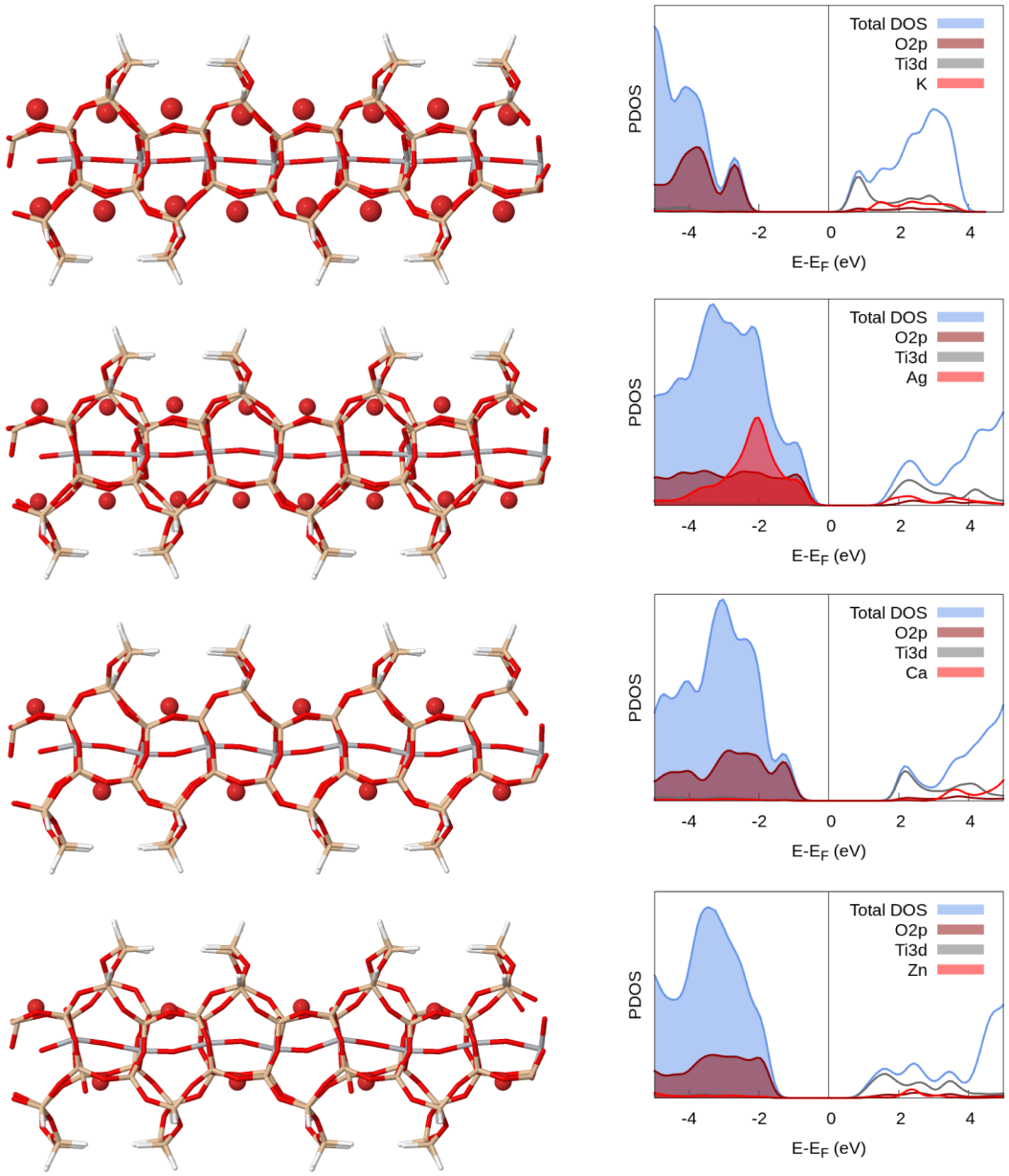

Figure 3. Full cationic exchange involving K^+, Ag^+, Ca^{2+}, and Zn^{2+} cations. Geometry optimized structures (left panels) are accompanied by the PDOS plots (right panels). The full spheres in the left panels represent the cations in an otherwise stick-drawn frame.

into a 100 mL of aqueous $AgNO_3$, $RuCl_3$, $AuCl_3$, $ZnSO_4{:}7H_2O$, and $CaCl_2{:}2H_2O$ solution of a given concentration, i.e., 1 M solution of metals salts. The solution was stirred vigorously for 24 h. After ion exchange, the samples were washed several times by centrifugation and dried at 70 °C in ambient air.

Inductively coupled plasma optical emission spectrometry (ICP-OES, PerkinElmer Optima 4300DV) was used for the elemental analysis. The ICP-OES determined Na, K, and M values (wt %) in the as-synthesized and full ion exchanged M-ETS-10 samples (M = Ag^+, Zn^{2+}, Ca^{2+}, Ru^{3+}, and Au^{3+}) are reported in Table 1. Upon ion exchange with Ag^+, Ru^{3+}, and Au^{3+}, the amount of Na^+ was reduced by 96%, 98%, and 96%, respectively. Although the degree of Na^+ exchange with Ca^{2+} and Zn^{2+} ions was somewhat lower, the Na^+ content of Ca-ETS-10 and Zn-ETS-10 samples was nonetheless considerably reduced by 65% and 81%, respectively. The decrease in K^+ content was instead lower, in line with previous ion-exchange experiments.[17]

Phase identification of all samples was done by X-ray powder diffraction (XRD) using Rigaku-Ultima IV XRD. The diffraction peaks were scanned between 5° and 40° with a scan speed of 1°/min. A Renishaw-type Raman microscope was utilized in the Raman spectroscopy analyses, where the excitation wavelength of 532 nm and a power of 0.5−1 mW were chosen for the acquisition.

3. RESULTS AND DISCUSSION

3.1. Na-ETS-10. Selected geometrical parameters for the two models of ETS-10 considered in this work are reported in Table 2 and compared with experimental[3,18,19] and theoretical values[4,5] from the literature. The optimized structures of the two models are very similar, pointing toward the robustness of the models; the O−Ti−O angles of the quantum wire are close to 180°, while the Ti−O−Ti angles are appreciably smaller. The computed values for both models are in reasonable

dx.doi.org/10.1021/jp503852t | J. Phys. Chem. C 2014, 118, 27281−27291

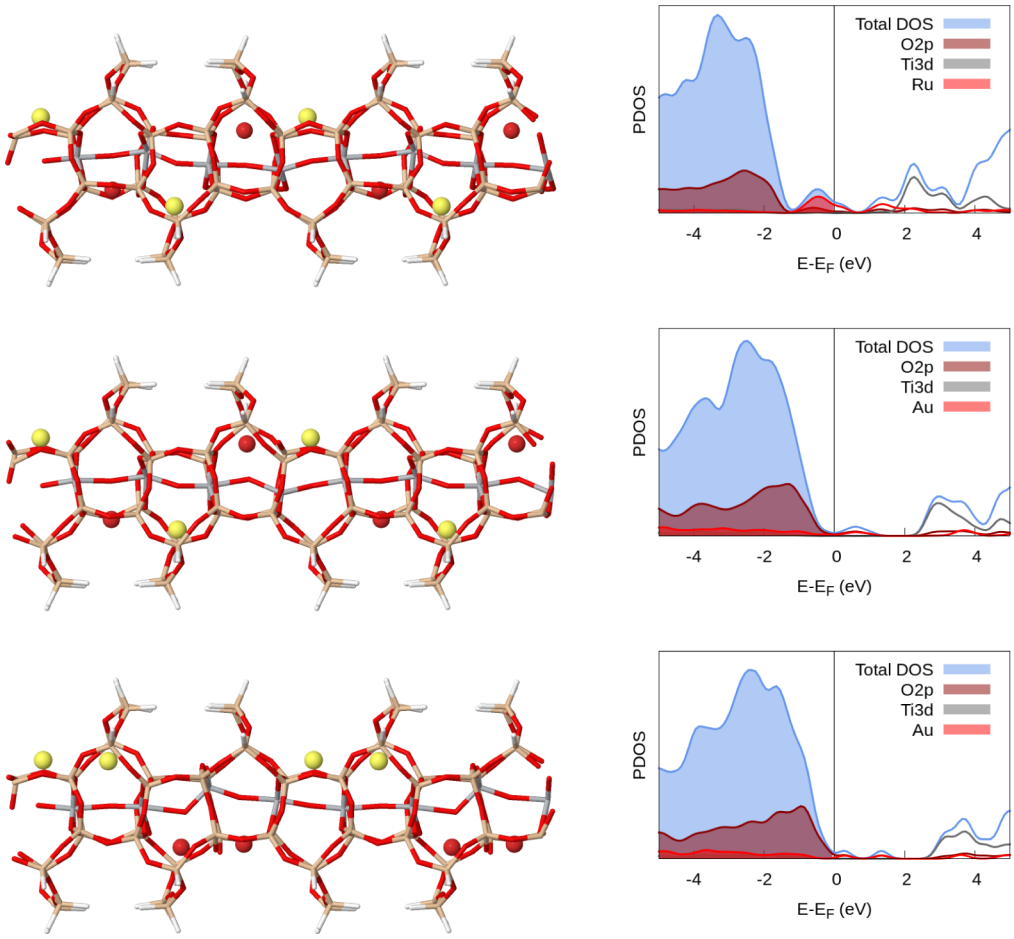

Figure 4. Full cationic exchange involving Ru^{3+} and Au^{3+}. The middle and bottom panels display the zigzag and dimer-like geometries for Au^{3+}. Geometry optimized structures (left panels) are accompanied by the PDOS plots (right panels). The full spheres in the left panels represent the cations (red) and the Na^+ ions (yellow) in an otherwise stick-drawn frame.

agreement with the values quoted by Zimmerman et al.[5] and closer to the experimental findings of Sankar et al.[18] when compared to the work of Damin et al.[4] It is also worth noting that both models predict a sequence of alternating long and short Ti−O bonds in the wire and confirm the EXAFS results of Sankar et al.[18] However, the predicted bond length difference is less pronounced (about 0.20 Å) compared to the value of about 0.40 Å as reported in ref 18. Our findings compare favorably with those of Zimmerman et al.[5] but are in disagreement with those of Damin et al.[4]

The present results support earlier findings of Damin et al.[4] concerning the geometry of the TiO_6 unit, with similar deviations from the ideal octahedral geometry. In particular, for model I, of the four O_{eq}−Ti−O_{eq} angles, two were in the range 83−85°, while the other two were in the range 95−97°, while the O_{eq}−Ti−O_{ap} angles were spread in the interval 85−95°. A similar pattern was detected in model II and for both models the Ti−O_{eq} bonds were in the range of 1.99−2.05 Å, in good agreement with previous results. Furthermore, the location of the Na^+ cations was in agreement with previous studies.[9] In our model, there are two distinct Na^+ species distinguishable by the slight difference in their distances to the nearest apical O atom. Na1−O1 and Na2−O1 distances reported are in the range 2.37−2.45 Å and 2.43−2.47 Å, respectively, for model II.

The partial charge on selected atoms for model II of ETS-10, resulting from a Bader charge analysis, are included in the Supporting Information, and we only provide a summary here. All Ti atoms are positively charged (about 2.2 |e|), while the oxygen atoms directly bonded to the Ti atoms have negative charges in the range −1.1 to −1.7 |e|, with the O_{ap} atoms less negatively charged than O_{eq}. The alternating long and short Ti−O bond pattern characterizing the wire does not affect the electron charge distribution among the O_{eq}. The variation of the negative partial charges on all other O atoms of the framework is very narrow.

As a tool for understanding electronic structure, in Figure 2, we report the total and partial density of states (PDOS) near the Fermi level for model II. In good agreement with the previous PDOS calculations,[4,5,8,15] the top of the valence band receives major contributions from the 2p orbitals of O_{ap} and O_{eq} atoms while the bottom of the conduction band is composed almost exclusively of contributions from the Ti 3d orbitals. The calculated band gap is 3.4 eV. This value is consistent with the DFT and TDDFT results of Zimmerman et al.,[5] who quoted a band gap value of about 3.10 eV, and the LDA-VWN gap of 3.22 eV reported by Damin et al.[4]

3.2. Ion-Exchanged M-ETS-10. In this section, we examine the structural and electronic properties of the ion-exchanged ETS-10 models, comparing them to those of the Na-form considered above. Two different cases are considered: a

dx.doi.org/10.1021/jp503852t | J. Phys. Chem. C 2014, 118, 27281−27291

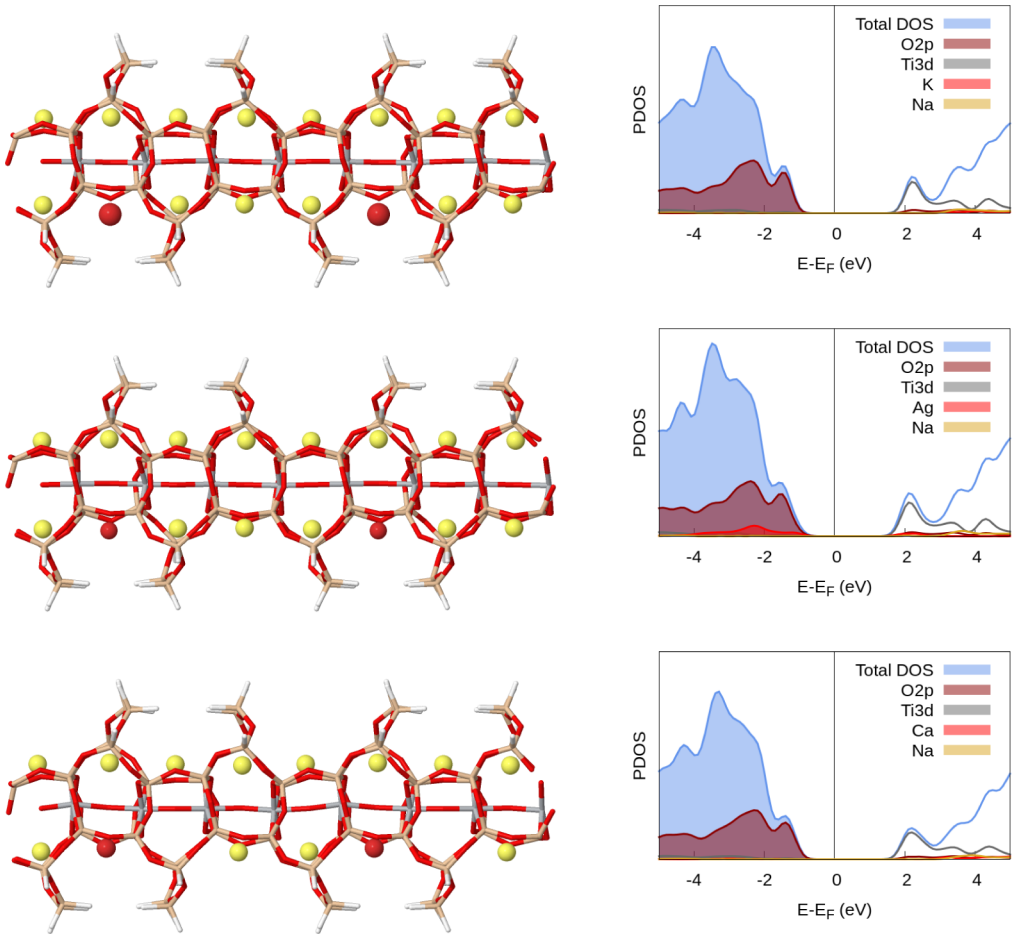

Figure 5. Partial cationic exchange involving K^+, Ag^+, and Ca^{2+} cations. Geometry optimized structures (left panels) are accompanied by the PDOS plots (right panels). The full spheres in the left panels represent the cations (red) and the Na^+ ions (yellow) in an otherwise stick-drawn frame.

partial cation exchange (one cation in each unit cell) and full cation exchange.

For the case of full cationic exchange, the site locations of K^+ and Ag^+ extraframework cations in the optimized structures are very similar to the corresponding Na-form, as can be seen in Figure 3. Analysis of the data reported in Table 3 reveals that compared to the Na-form, in the K-form there is a slightly smaller asymmetry in the Ti−O_{ap} bonds while the Ag^+ ion gives rise to a smaller asymmetry in consecutive bond angles. The exchange of Na^+ ions with Ca^{2+} affects mostly the Ti−O−Ti bond angles, while the bond lengths remain close to those of the Na-form. On the other hand, sizable distortions are observed for the Zn^{2+} cation (bottom panel of Figure 3). In fact, while the pattern of alternating long and short Ti−O bonds are still preserved for Zn^{2+}, their difference in length increases from 0.22 Å in the Na-form to a maximum value of about 0.36 Å (Table 3) in the Zn-form. These changes in bond geometry occur so as to accommodate the zigzag buckled O−Ti−O bond configuration caused by the location of the cations. The extent to which this buckling occurs in the Zn form can be seen from the O−Ti−O and Ti−O−Ti angles listed in Table 3 and can also be visually observed in Figure 3. Among all the cations studied, Ru^{3+} and Au^{3+} are those that cause the largest distortion in the wire. In both cases, the bond lengths display large deviations with respect to the Na-form and do not follow a well-defined pattern of long−short Ti−O distances as was observed for the other cations. Similar observations apply to the bond angles. In the case of Au dimer, the distortion is large enough that there are indications of rupture in the wire. The large distortion in this case stems from the fact that one of the Au cations forms a planar AuO_4 unit with the surrounding equatorial oxygens. This unit is reminiscent of the AuO_4 units in the crystalline auric oxide, Au_2O_3,[41] with similar Au−O distances (∼2.0 Å). One O atom of this unit is shared by the other Au atom, which in turn interacts with two other O atoms in its coordination sphere. As a consequence, the Ti2 atom is tetrahedrally coordinated with O ligands. Ru^{3+} and zigzag Au^{3+} display similar distortion patterns. Unlike the dimer-like Au^{3+} configuration, there are five oxygens in their coordination sphere, four O_{eq} of neighboring TiO_6 units, and one apical oxygen.

In summary, with reference to the data reported in Table 3, we conclude that the presence of two inequivalent Ti−O bonds along the quantum wire is conserved upon full cationic exchange of Na^+ with all ions considered except Ru^{3+} and Au^{3+}. The distortions caused by Ca^{2+} and Zn^{2+} ions, while noticeable, protect the integrity of the wire.

Upon partial ion exchange of Na^+ with K^+ and Ag^+, the structural parameters of the wire are only slightly altered, as can be seen from the data reported in Table 4, and this observation is consistent with previous experimental results.[13] Insertion of Ca^{2+} affects only the bond distances and angles of the portion of the wire in proximity to the cation. Although the inclusion of a single Ru^{3+} or Au^{3+} cation causes only a minor structural

dx.doi.org/10.1021/jp503852t | J. Phys. Chem. C 2014, 118, 27281−27291

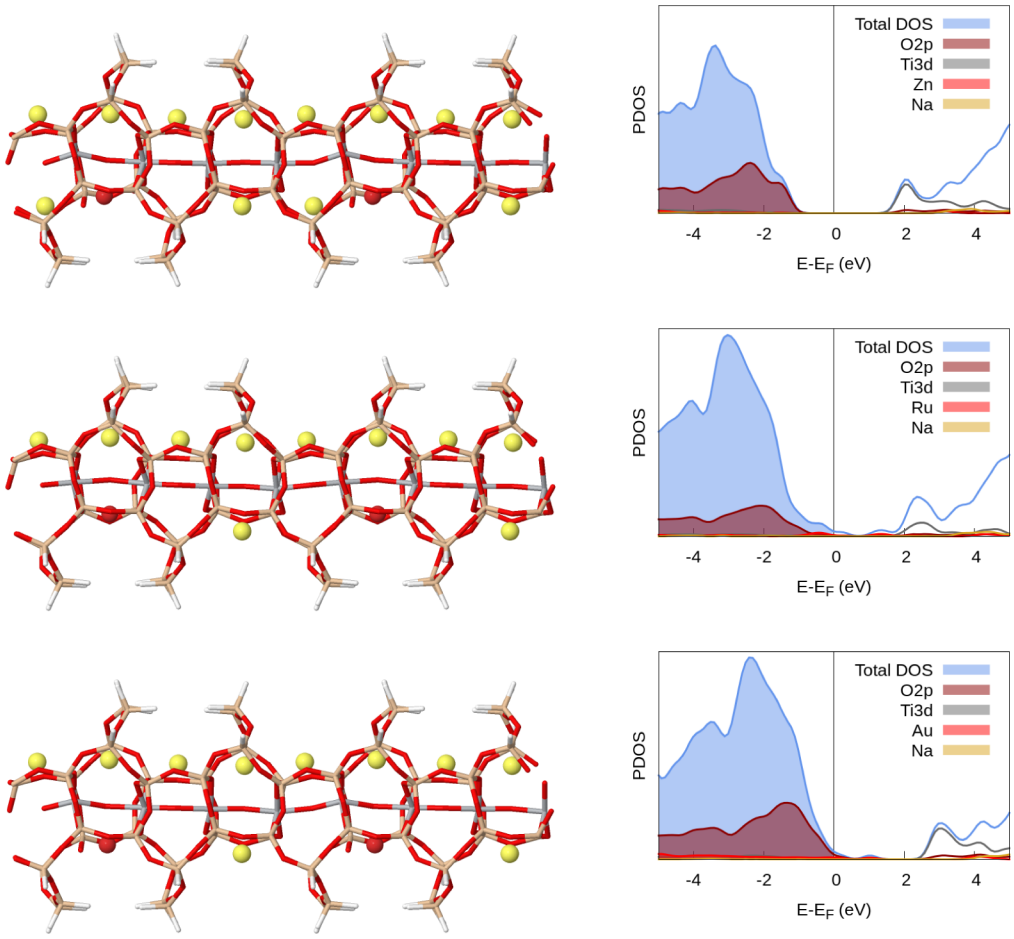

Figure 6. Partial cationic exchange involving Zn^{2+}, Ru^{3+}, and Au^{3+} cations. Geometry optimized structures (left panels) are accompanied by the PDOS plots (right panels). The full spheres in the left panels represent the cations (red) and the Na^+ ions (yellow) in an otherwise stick-drawn frame.

Table 1. ICP-OES-Determined Na, K, and M Values (wt %) of As-Synthesized (Na,K)-ETS-10 and Full Ion-Exchanged ETS-10 (M-ETS-10, where M = Ag^+, Zn^{2+}, Ca^{2+}, Ru^{3+}, and Au^{3+}) Samples

sample	Na	K	M
(Na,K)-ETS-10	6.05 ± 0.04	3.65 ± 0.02	
Ag-ETS-10	0.23 ± 0.01	2.01 ± 0.04	25.5 ± 0.10
Ca-ETS-10	2.13 ± 0.04	2.11 ± 0.01	4.45 ± 0.04
Zn-ETS-10	1.17 ± 0.06	2.36 ± 0.06	8.87 ± 0.04
Ru-ETS-10	0.15 ± 0.01	1.44 ± 0.06	9.23 ± 0.10
Au-ETS-10	0.22 ± 0.02	1.55 ± 0.06	7.46 ± 0.16

distortion of the wire, the bond length pattern characteristic of the wire is somewhat lost. This suggests that even a small concentration of Ru^{3+} and Au^{3+} may cause large distortions.

We now turn our attention to the trend in the partial charges, reported in Table 5 (and Supporting Information) for the case of full and partial ion exchange. An exchange of 1/8 of the Na^+ ions with K^+ ions does not have any noticeable effect on the charge distribution of the TiO_6 unit, the remaining Na^+ ions and the O atoms of the insulating silica matrix, indicating that the interaction of Na^+ and the ETS-10 framework is not affected by this substitution. The partial positive charge on K^+ is somewhat higher than on Na^+. Similar conclusions can be reached after examination of the results obtained for partial exchange with Ag^+ ions. Here however the partial charge of Ag^+ is slightly lower. The Ca^{2+} ions acquire a positive charge of approximately 1.6 |e|, while the charge on Zn^{2+} is about 1.3 |e|. Finally, both Ru^{3+} and Au^{3+} acquire a comparatively small amount of charge, indicating a tendency toward a lower oxidation state. This is true especially for Au^{3+}. In particular, when Au^{3+} and Ru^{3+} are incorporated in the framework, we observe a charge transfer from the oxygen atoms belonging to the coordination sphere of the cation. The charge transfer and the consequent strong perturbation of the electron density distribution are thus intimately connected to the structural deformations of the wire. Similar observations also apply to the full ion exchange as seen in Table 5.

In addition to the structural parameters, ion exchange can potentially induce changes in the electronic structure. If the modifications caused by each cation to the ETS-10 system are well characterized, the ion-exchange mechanism may be used as a viable tool to tune the electronic properties of the system. To this end, we report the density of states (DOS) of the entire system along with the PDOS of the Ti 3d, O 2p (apical and equatorial combined), and states of the metal ions in Figures 3 and 4 for the full exchange case. DOS and PDOS plots for partially exchanged systems are instead displayed in Figures 5 and 6. In the case of the fully exchanged K-form, the contribution of the K-states near the Fermi level is negligible and consequently the band gap is still characteristically determined by the Ti 3d and O 2p states. Ag^+ derived states, on the other hand, make sizable contributions to the valence

dx.doi.org/10.1021/jp503852t | J. Phys. Chem. C 2014, 118, 27281−27291

Table 2. Selected Structural Parameters of the Two Models of ETS-10 Employed in This Work, and Comparison with Theoretical and Experimental Data from the Literature[a]

						present work	
	EXAFS[19]	XRD[3]	EXAFS[18]	Zimmerman et al.[5]	Damin et al.[4]	model I	model II
Ti1−Ti2	3.73	3.743	3.76	3.74	3.759	3.71	3.69
Ti1−O1	1.87(1)	1.872(1)	1.71	1.89	1.883	1.79	1.78
Ti1−O2	1.87(1)	1.872(1)	2.11	1.97	1.883	1.99	2.00
Ti2−O1				1.94		1.98	2.00
Ti2−O3				1.96		1.78	1.78
Ti3−O2				1.86		1.78	1.78
Ti3−O4				2.07		1.98	2.00
Ti1−O5	2.05(1)	1.99(1)	2.02	1.99−2.02	2.00	2.01−2.03	1.98−2.05
Ti2−O6				1.92−2.09		1.99−2.05	2.00−2.05
Ti3−O7				1.91−2.13		1.99−2.05	2.00−2.04
Ti1−O8	3.78(2)	3.74		3.53−3.56	3.5	3.51−3.58	3.46−3.53
Ti1−O6	4.10(3)	4.17		3.84−4.42	4.05−4.15	3.85−4.39	3.93−4.26
Ti1−O9	4.22(3)	4.23−4.25		3.92−4.54	4.18−4.33	4.06−4.24	4.05−4.25
Ti1−Si1	3.32	3.27	3.31	3.20−3.31	3.26−3.27	3.21−3.29	3.16−3.26
Ti1−Na1	3.05(2)	3.15−3.20	3.07	3.07−3.14	2.976	2.99	3.04
O5−Si1	1.60(2)	1.61	1.63	1.64−1.65	1.61−1.62	1.63	1.62−1.63
Na1−O1					2.47	2.37−2.38	2.37−2.45
Na2−O1					2.49	2.41	2.43−2.47
Ti1−O1−Ti2	180(5) ± 30	177.9	165	157.7	172.6	159.4	156.1
Ti1−O2−Ti3				152.6		160.0	157.8
Ti1−O5−Si1	132(5) ± 15	130.2	130	122.4−128.8	128.6−129.8	123.5−128.8	122.6−127.5

[a]Bond lengths are in Å and angles in deg. For the atomic labeling, we refer to Figure 1. Only the parameters corresponding to the asymmetric model of Zimmerman et al.[5] are included in the comparison.

Table 3. Structural Properties of the Quantum Wire in the Fully Ion-Exchanged M-ETS-10, Model II[a]

M-ETS-10	Na^+	K^+	Ag^+	Ca^{2+}	Zn^{2+}	Ru^{3+}	Au^{3+} (zigzag)	Au^{3+} (dimer)
O3−Ti2	1.78	1.78	1.77	1.75	1.78	2.06	2.19	1.74
O1−Ti2	2.00	1.96	2.01	2.00	2.06	1.83	1.82	1.93
O1−Ti1	1.78	1.79	1.77	1.74	1.76	1.82	1.85	2.33
O2−Ti1	2.01	1.97	2.07	2.04	2.12	1.93	1.98	1.74
O2−Ti3	1.78	1.78	1.77	1.74	1.76	2.04	2.02	1.99
O4−Ti3	2.00	1.95	2.02	2.02	1.96	1.83	1.82	1.94
O4−Ti4	1.77	1.77	1.76	1.74	1.79	1.82	1.84	1.75
O3−Ti2−O1	174.1	172.2	160.1	164.1	165.8	176.0	162.6	117.3
Ti2−O1−Ti1	156.1	166.3	153.6	164.6	160.4	150.1	147.6	134.2
O1−Ti1−O2	178.8	174.8	169.1	168.3	168.4	148.4	153.0	168.9
Ti1−O2−Ti3	157.8	167.7	159.4	170.7	166.9	161.4	163.9	169.1
O2−Ti3−O4	175.3	172.1	164.5	165.3	144.7	175.9	155.5	169.5
Ti3−O4−Ti4	161.8	170.3	167.0	171.9	157.7	156.3	153.6	173.6

[a]Bond lengths are in Å and angles in deg. For the atomic labeling, we refer to Figure 1.

band without, however, causing any noticeable changes to the band gap. The inclusion of both Ca^{2+} and Zn^{2+} leave the band structure largely unchanged, making no contributions around the Fermi energy. The behavior of Ru^{3+} and Au^{3+}, however, is significantly different. Ru^{3+} contributes a large peak centered around the Fermi energy, while the presence of Au^{3+} introduces gap states. Furthermore, in both cases, the extent of Ti 3d and O 2p contributions are also altered.

As expected, changes to the electronic structure are much less pronounced in the partial exchange case. While K^+, Ca^{2+}, and Zn^{2+} introduce no contribution to the PDOS for energies close to the Fermi level, Ag^+ donates a small number of states to the tail of the valence band without affecting the gap. Au^{3+} lowers the Fermi level to slightly below the top of the valence band, while Ru^{3+}, as in the case of the full-exchange, introduces a peak at the Fermi level as a result of its interaction with the apical oxygens. The generally relatively small changes to the band gap due to ion exchange is consistent with the experimental observation in ref.[6]

To test the crystallinity of the material upon ion-exchange XRD data was collected from all samples. The as-synthesized ETS-10 crystals, which in their native form contain a mixture of Na^+ and K^+ counterions, were used as the host material for ion-exchanged samples (M-ETS-10). According to the XRD patterns of the as-synthesized ETS-10 and M-ETS-10 samples (M = Ag^+, Zn^{2+}, Ca^{2+}, Ru^{3+}), there was no noticeable change in the positions of the Bragg peaks as shown in Figure 7. Powder XRD patterns of the ion-exchanged ETS-10 samples look similar to the as-synthesized ETS-10. This suggests that the crystal structures remain unperturbed by the ion-exchange. The crystallinity of the samples was calculated from XRD data and was found to decrease for M-ETS-10 (i.e., 68%, 71%, 90%, 53%,

dx.doi.org/10.1021/jp503852t | J. Phys. Chem. C 2014, 118, 27281−27291

Table 4. Structural Properties of the Quantum Wire in the Partially Ion-Exchanged M-ETS-10, Model II[a]

M-ETS-10	K^+	Ag^+	Ca^{2+}	Zn^{2+}	Ru^{3+}	Au^{3+}
O3−Ti2	1.78	1.78	1.98	2.02	1.82	1.82
O1−Ti2	1.98	1.99	1.83	1.87	1.93	2.02
O1−Ti1	1.79	1.78	1.84	1.81	1.72	1.72
O2−Ti1	1.99	1.99	1.93	2.04	2.09	2.20
O2−Ti3	1.77	1.78	1.94	1.86	2.08	1.91
O4−Ti3	2.01	1.98	1.79	1.76	1.72	1.74
O4−Ti4	1.76	1.77	2.00	2.05	1.92	1.93
O3−Ti2−O1	174.3	174.4	176.5	174.3	174.5	176.3
Ti2−O1−Ti1	157.7	155.1	157.0	155.5	157.4	158.1
O1−Ti1−O2	177.7	176.1	176.1	168.7	175.1	177.6
Ti1−O2−Ti3	158.9	159.0	162.3	159.0	163.8	148.7
O2−Ti3−O4	176.4	171.2	166.5	140.2	170.8	139.2
Ti3−O4−Ti4	162.4	166.9	162.5	159.4	164.3	164.9

[a]Bond lengths are in Å and angles in deg. For the atomic labeling, we refer to Figure 1.

Table 5. Bader Charge Analysis for the Cations in the Fully and Partially Exchanged M-ETS-10, Model II (M = Na^+, K^+, Ag^+, Ca^{2+}, Zn^{2+}, Ru^{3+}, and Au^{3+})[a]

	full	partial
Na^+	0.9	
K^+	1.0	1.0
Ag^+	0.7	0.7
Ca^{2+}	1.6	1.6
Zn^{2+}	1.3	1.3
Ru^{3+}	1.5	1.5
Au^{3+} (zigzag)	1.1−1.2	1.1
Au^{3+} (dimer)	1.2−1.3	

[a]Values are in units of |e|.

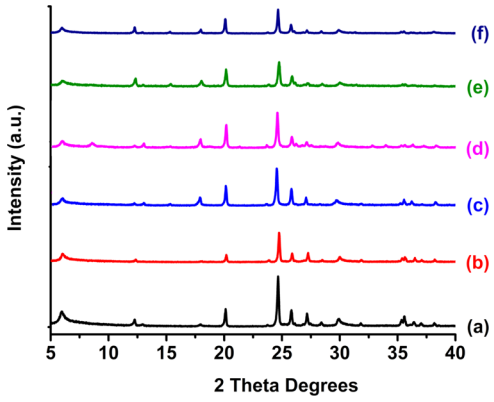

Figure 7. XRD patterns of (Na,K)-ETS-10 (a) and ion-exchanged ETS-10 (M-ETS-10, where M = Ag^+ (b), Ca^{2+} (c), Zn^{2+} (d), Ru^{3+} (e), and Au^{3+} (f)).

50% for Ag^+, Zn^{2+}, Ca^{2+}, Ru^{3+}, and Au^{3+}, respectively) with respect to the as-synthesized ETS-10 sample, with the largest change observed for Ru- and Au-ETS-10 samples. Nevertheless, the morphologies were identical with respect to the original sample in all M-ETS-10 samples.

To elucidate the effect of ion-exchange on the local structural deformations induced into the Ti−O−Ti wire, Raman spectra were taken for only the fully ion-exchanged M-ETS-10 samples. Figure 8 shows the Raman spectra of ETS-10 and M-ETS-10. The intense band at around 724−729 cm^{-1} dominates the spectrum of ETS-10 and has been previously assigned to the Ti−O stretch of the Ti−O−Ti chains.[11,13,17] As shown in

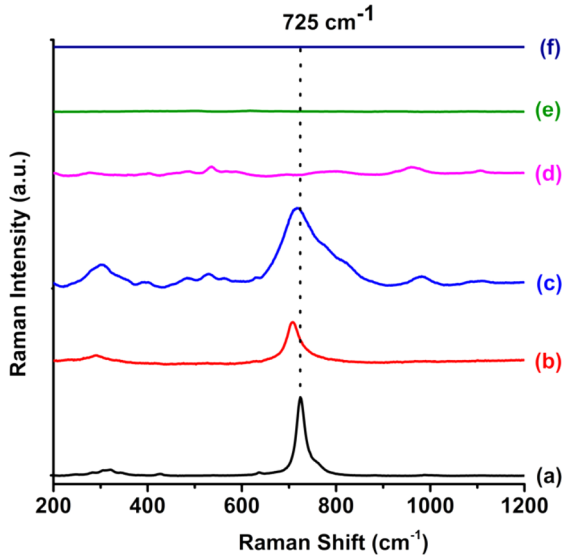

Figure 8. Raman spectra of (Na,K)-ETS-10 (a) and ion-exchanged ETS-10 (M-ETS-10, where M = Ag^+ (b), Ca^{2+} (c), Zn^{2+} (d), Ru^{3+} (e), and Au^{3+} (f)).

Figure 8, for Ca^{2+} and Ag^+, this band is significantly broadened and slightly shifted toward the lower frequency region, respectively, with an additional loss in intensity for Ag^+. Similar behaviors were also observed for damaged Ti−O−Ti chains in ETS-10 upon ion-exchange, which are in correlation with this study.[11,17] When M = Zn^{2+}, Ru^{3+}, and Au^{3+}, the characteristic band completely disappears, indicating a partial or entire disruption of this wire, leading to the decrease in the Ti−O stretching. These results suggest that the most significant structural changes to the Ti−O−Ti wire are induced upon Na^+ exchange with M = Zn^{2+}, Au^{3+}, and Ru^{3+}, while less pronounced damages are caused upon M = Ca^{2+} and Ag^+ insertion. These observations fully agree with our computational results. In particular, our results strongly suggest that the disappearance of the Ti−O stretching peak in the case of Au^{3+} and Ru^{3+} can be attributed to the large structural distortions in the Ti−O−Ti wires.

4. CONCLUSIONS

Understanding the extent of structural distortions caused by ion exchange is important in tuning ETS-10 for the particular

dx.doi.org/10.1021/jp503852t | J. Phys. Chem. C 2014, 118, 27281−27291

application at hand. DFT calculations within the GGA were carried out on two models of ETS-10 together with XRD and Raman spectroscopy experiments, with the aim to elucidate the effect of ion exchange on the structural, electronic, and vibrational properties of the Ti−O−Ti quantum wire.

The two ETS-10 models considered include some framework silicon and oxygen atoms in addition to the core Ti−O−Ti wire atoms. The similarity of the calculated structural paramaters such as distances and angles in the two models and their agreement with previous works validates our use of the models. In our calculations, Ti−O bond distances and bond angles were taken to be the figure of merit for the extent of the distortion of the Ti−O−Ti wire. Our DFT calculations confirm the presence of two inequivalent Ti−O bonds along the chain in the Na-form, in agreement with past theoretical and experimental studies. Our calculations also indicate that K^+, Ag^+, and Ca^{2+} cause minor distortions to the wire upon full cation exchange, while Zn^{2+}, Au^{3+}, and Ru^{3+} trigger extensive structural changes with respect to the Na-form. The distortion patterns are interpreted and rationalized by means of charge transfer between the metal and the framework.

Partial ion exchange was also investigated. In this case, structural properties remain closer to those calculated for the Na^+ form. However, indications of large distortions are already detected for Au^{3+} and Ru^{3+}. In spite of the low concentration of the cation, the DOS plots of the partially exchanged systems already reveal visible changes to the band gap in the cases of Ru^{3+} and Au^{3+} ions.

In the experimental portion of this work, following the synthesis and characterization of the Na-form of ETS-10, ion exchange with alkali, earth-alkaline, and transition metal cations was performed and characterized by ICP-OES. Our XRD data reveal a reduction in crystallinity for Ru^{3+} and Au^{3+}, while for all other ions no large changes were observed. Raman spectroscopic analysis of the Na-form and M-ETS-10 reveal a very close correlation between the extent of the structural distortion and the peak intensity of the Ti−O bond stretching mode between 724 and 729 cm^{-1}. While the peak is clearly visible in Na^+, Ag^+, and Ca^{2+}, it is completely absent in the Zn^{2+}, Au^{3+}, and Ru^{3+}-exchanged ETS-10, indicating large distortion in the wire. These observations are fully supported by the theoretical results.

■ ASSOCIATED CONTENT

Ⓢ Supporting Information

Bader charges for selected atoms in fully and partially exchanged M-ETS-10. This material is available free of charge via the Internet at http://pubs.acs.org.

■ AUTHOR INFORMATION

Corresponding Authors

*For D.T.: E-mail, dtoffoli@metu.edu.tr.
*For H.U.: E-mail, ustunel@metu.edu.tr.
*For B.A.: E-mail, akata@metu.edu.tr.

Notes

The authors declare no competing financial interest.

■ ACKNOWLEDGMENTS

We thank ULAKBIM-TRGRID for computational resources. The support provided by METU-Central Laboratory is also acknowledged.

■ REFERENCES

(1) Kuznicki, S. M. Large-Pored Crystalline Titanium Molecular Sieve Zeolites. U.S. Patent US 4853202 A, 1989.
(2) Anderson, M. W.; Terasaki, O.; Ohsuna, T.; Philippou, A.; MacKay, S. P.; Ferreira, A.; Rocha, J.; Lidin, S. Structure of the Microporous Titanosilicate ETS-10. *Nature* **1994**, *367*, 347−351.
(3) Wang, X.; Jacobson, A. J. Crystal Structure of the Microporous Titanosilicate ETS-10 Refined from Single Crystal X-Ray Diffraction Data. *Chem. Commun.* **1999**, *612*, 973−974.
(4) Damin, A.; Xamena, F. X. L; Civalleri, B.; Zicovich-Wilson, C. M.; Zecchina, A. Structural, Electronic, and Vibrational Properties of the Ti−O−Ti Quantum Wires in the Titanosilicate ETS-10. *J. Phys. Chem. B* **2004**, *108*, 1328−1336.
(5) Zimmerman, A. M.; Doren, D. J.; Lobo, R. F. Electronic and Geometric Properties of ETS-10: QM/MM Studies of Cluster Models. *J. Phys. Chem. B* **2006**, *110*, 8959−8964.
(6) Lamberti, C. Electron-Hole Reduced Effective Mass in Monoatomic ...−O−Ti−O−Ti−O−... Quantum Wires Embedded in the Siliceous Crystalline Matrix of ETS-10. *Microporous Mesoporous Mater.* **1999**, *30*, 155−163.
(7) Jeong, N. C.; Lee, M. H.; Yoon, K. B. Length-Dependent Band-Gap Shift of TiO_3^{2-} Molecular Wires Embedded in Zeolite ETS-10. *Angew. Chem., Int. Ed.* **2007**, *46*, 5868−5872.
(8) Ching, W. Y.; Xu, Y.-N.; Gu, Z.-Q. Structure and Properties of Microporous Titanosilicate Determined by First-Principles Calculations. *Phys. Rev. B* **1996**, *54*, R15585−R15589.
(9) Grillo, M.; Carrazza, J. Computational Modeling of the Nonframework Cation Location and Distribution in Microporous Titanosilicate ETS-10. *J. Phys. Chem.* **1996**, *100*, 12261−12264.
(10) Anderson, M. W.; Agger, J. R.; Luigi, D.-P.; Baggaley, A. K.; Rocha, J. Cation Sites in ETS-10: ^{23}Na 3Q MAS NMR and Lattice Energy Minimisation Calculations. *Phys. Chem. Chem. Phys.* **1999**, *1*, 2287−2292.
(11) Pavel, C. C.; Zibrowius, B.; Löffler, E.; Schmidt, W. On the Influence of Ion Exchange on the Local Structure of the Titanosilicate ETS-10. *Phys. Chem. Chem. Phys.* **2007**, *9*, 3440−3446.
(12) Krisnandi, Y. K.; Lachowski, E. E.; Howe, R. F. Effects of Ion Exchange on the Structure of ETS-10. *Chem. Mater.* **2006**, *18*, 928−933.
(13) Galioğlu, S.; Zahmakran, M.; Kalay, Y. E.; Özkar, S.; Akata, B. Effect of Silver Encapsulation on the Local Structure of Titanosilicate ETS-10. *Microporous Mesoporous Mater.* **2012**, *159*, 1−8.
(14) Xu, Y.-N.; Ching, W. Y.; Gu, Z.-Q. Electronic Structure of Microporous Titanosilicate ETS-10. *Ferroelectrics* **1997**, *194*, 219−226.
(15) Bordiga, S.; Turnes Palomino, G.; Zecchina, A.; Ranghino, G.; Giamello, E.; Lamberti, C. Stoichiometric and Sodium-Doped Titanium Silicate Molecular Sieve Containing Atomically Defined −OTiOTiO− Chains: Quantum ab Initio Calculations, Spectroscopic Properties, and Reactivity. *J. Chem. Phys.* **2000**, *112*, 3859−3867.
(16) Yilmaz, B.; Warzywoda, J.; Sacco, A. Spectroscopic Characterization of the Quantum Wires in Titanosilicates ETS-4 and ETS-10. *Nanotechnology* **2006**, *17*, 4092−4099.
(17) Jeong, N. C.; Lee, Y. J.; Park, J.-H.; Lim, H.; Shin, C.-H.; Cheong, H.; Yoon, K. B. New Insights into ETS-10 and Titanate Quantum Wire: A Comprehensive Characterization. *J. Am. Chem. Soc.* **2009**, *131*, 13080−13092.
(18) Sankar, G.; Bell, R. G.; Thomas, J. M.; Anderson, M. W.; Wright, P. A. Determination of the Structure of Distorted TiO_6 Units in the Titanosilicate ETS-10 by a Combination of X-ray Absorption Spectroscopy and Computer Modeling. *J. Phys. Chem.* **1996**, *100*, 449−452.
(19) Prestipino, C.; Solari, P. L.; Lamberti, C. EXAFS and XANES Investigation of the ETS-10 Microporous Titanosilicate. *J. Phys. Chem. B* **2005**, *109*, 13132−13137.
(20) Shough, A. M.; Doren, D. J.; Ogunnaike, B. Transition Metal Substitution in ETS-10: DFT Calculations and a Simple Model for Electronic Structure Prediction. *Chem. Mater.* **2009**, *21*, 1232−1241.

(21) Borello, E.; Lamberti, C.; Bordiga, S.; Zecchina, A.; Arean, C. O. Quantum-Size Effects in the Titanosilicate Molecular Sieve. *Appl. Phys. Lett.* **1997**, *71*, 2319−2321.
(22) Philippou, A.; Anderson, M. W. Aldol-Type Reactions over Basic Microporous Titanosilicate ETS-10 Type Catalysts. *J. Catal.* **2000**, *189*, 395−400.
(23) Valente, A.; Lin, Z.; Brandão, P.; Portugal, I.; Anderson, M.; Rocha, J. Gas-Phase Oxidative Dehydrogenation of Cyclohexanol over ETS-10 and Related Materials. *J. Catal.* **2001**, *200*, 99−105.
(24) Doskocil, E. J. Effect of Water and Alkali Modifications on ETS-10 for the Cycloaddition of CO_2 to Propylene Oxide. *J. Phys. Chem. B* **2005**, *109*, 2315−2320.
(25) Usseglio, S.; Calza, P.; Damin, A.; Minero, C.; Bordiga, S.; Lamberti, C.; Pelizzetti, E.; Zecchina, A. Tailoring the Selectivity of Ti-Based Photocatalysts (TiO_2 and Microporous ETS-10 and ETS-4) by Playing with Surface Morphology and Electronic Structure. *Chem. Mater.* **2006**, *18*, 3412−3424.
(26) Waghmode, S. B.; Vetrivel, R.; Hegde, S. G.; Gopinath, C. S.; Sivasanker, S. Physicochemical Investigations of the Basicity of the Cation Exchanged ETS-10 Molecular Sieves. *J. Phys. Chem. B* **2003**, *107*, 8517−8523.
(27) Lopes, C.; Otero, M.; Coimbra, J.; Pereira, E.; Rocha, J.; Lin, Z.; Duarte, A. Removal of Low Concentration Hg^{2+} from Natural Waters by Microporous and Layered Titanosilicates. *Microporous Mesoporous Mater.* **2007**, *103*, 325−332.
(28) Atienzar, P.; Valencia, S.; Corma, A.; García, H. Titanium-Containing Zeolites and Microporous Molecular Sieves as Photovoltaic Solar Cells. *ChemPhysChem* **2007**, *8*, 1115−1119.
(29) Galioglu, S.; Isler, M.; Demircioglu, Z.; Koc, M.; Vocanson, F.; Destouches, N.; Turan, B.; Akata, R. 8. Photochromic Behavior of Silver Nanoparticle Incorporated Titanosilicate ETS-10 Films. *Microporous Mesoporous Mater.* **2014**, *196*, 136−144.
(30) Southon, P. D.; Howe, R. F. Spectroscopic Studies of Disorder in the Microporous Titanosilicate ETS-10. *Chem. Mater.* **2002**, *14*, 4209−4218.
(31) Pavel, C. C.; Park, S.-H.; Dreier, A.; Tesche, B.; Schmidt, W. Structural Defects Induced in ETS-10 by Postsynthesis Treatment with H_2O_2 Solution. *Chem. Mater.* **2006**, *18*, 3813−3820.
(32) Hohenberg, P.; Kohn, W. Inhomogeneous Electron Gas. *Phys. Rev.* **1964**, *136*, B864−B871.
(33) Kohn, W.; Sham, L. J. Self-Consistent Equations Including Exchange and Correlation Effects. *Phys. Rev.* **1965**, *140*, A1133−A1138.
(34) Vanderbilt, D. Soft Self-Consistent Pseudopotentials in a Generalized Eigenvalue Formalism. *Phys. Rev. B* **1990**, *41*, 7892−7895.
(35) Perdew, J. P.; Burke, K.; Ernzerhof, M. Generalized Gradient Approximation Made Simple. *Phys. Rev. Lett.* **1996**, *77*, 3865−3868.
(36) Giannozzi, P.; Baroni, S.; Bonini, N.; Calandra, M.; Car, R.; Cavazzoni, C.; Ceresoli, D.; Chiarotti, G. L.; Cococcioni, M.; Dabo, I.; et al. QUANTUM ESPRESSO: A Modular and Open-Source Software Project for Quantum Simulations of Materials. *J. Phys.: Condens. Mater.* **2009**, *21*, 395502.
(37) Kokalj, A. Computer Graphics and Graphical User Interfaces as Tools in Simulations of Matter at the Atomic Scale. *Comput. Mater. Sci.* **2003**, *28*, 155−168.
(38) Hanson, R. M.; Prilusky, J.; Renjian, Z.; Nakane, T.; Sussman, J. L. JSmol and the Next-Generation Web-Based Representation of 3D Molecular Structure as Applied to Proteopedia. *Isr. J. Chem.* **2013**, *53*, 207−216.
(39) Monkhorst, H. J.; Pack, J. D. Special Points for Brillouin-Zone Integrations. *Phys. Rev. B* **1976**, *13*, 5188−5192.
(40) Henkelman, G.; Arnaldsson, A.; Jónsson, H. A Fast and Robust Algorithm for Bader Decomposition of Charge Density. *Comput. Mater. Sci.* **2006**, *36*, 354−360.
(41) Shi, H.; Asahi, R.; Stampfl, C. Properties of the Gold Oxides Au_2O_3 and Au_2O: First-Principles Investigation. *Phys. Rev. B* **2007**, *75*, 205125.